

to appear in *Advances in Solid State Physics*, ed. by B. Kramer (Springer 2001)

Transport in nanostructures: A comparison between nonequilibrium Green functions and density matrices

Andreas Wacker

Institut für Theoretische Physik, Technische Universität Berlin,
Hardenbergstr. 36, 10623 Berlin, Germany

Abstract. Stationary electric transport in semiconductor nanostructures is studied by the method of nonequilibrium Green functions. In the case of sequential tunneling the results are compared with density matrix theory, providing almost identical results. Nevertheless, the method of Green functions is easier to handle due to the availability of an absolute energy scale. It is demonstrated, that the transport in complicated structures, like quantum cascade lasers, can be described in reasonable agreement with experiment.

1 Introduction

Transport through semiconductor nanostructures[1,2,3] is dominated by quantum effects. A corresponding quantum transport theory can be based on density matrices or nonequilibrium Green functions (see, e.g., Refs. [4,5] and references cited therein). In this article, I want to show that nonequilibrium Green functions provide a strong tool to handle this situation for *stationary* transport, even for complicated structures like the quantum cascade laser. By a direct comparison with the density matrix method the differences between both methods are examined for the test case of sequential tunneling between neighboring quantum wells.

The article is organized as follows: After a general formulation of the problem (Section 2) it will be shown in Section 3 how the method of nonequilibrium Green functions can be applied in the stationary state. A simple example is discussed in detail in Section 4, and a direct comparison with density matrix theory is made in Section 5. Finally, the full power of the Green function approach is demonstrated in a simulation of quantum cascade lasers in Section 6.

2 General aspects of quantum transport

The starting point for a quantum kinetic description is the Hamilton operator in second quantisation (using basis states labeled by α)

$$\hat{H} = \hat{H}_0 + \hat{U} + \hat{H}_{\text{scatt}} \quad (1)$$

where (in Heisenberg representation)

$$\hat{H}_0 = \sum_{\alpha} E_{\alpha} a_{\alpha}^{\dagger}(t) a_{\alpha}(t) \quad (2)$$

is diagonal in the basis $|\alpha\rangle$,

$$\hat{U} = \sum_{\alpha, \beta} U_{\alpha, \beta}(t) a_{\alpha}^{\dagger}(t) a_{\beta}(t) \quad (3)$$

describes nondiagonal parts of the Hamiltonian as well as the presence of electric fields, and \hat{H}_{scatt} refers to interactions with phonons, random impurity potentials (which are treated within impurity averaging), or interactions between the particles. The final goal is to calculate various observables such as the occupation of the state α

$$f_{\alpha}(t) = \langle a_{\alpha}^{\dagger}(t) a_{\alpha}(t) \rangle \quad (4)$$

or transition rates

$$j^{\beta \rightarrow \alpha}(t) = \frac{2}{\hbar} \Re \left\{ i U_{\beta, \alpha} \langle a_{\beta}^{\dagger}(t) a_{\alpha}(t) \rangle \right\} \quad (5)$$

between the respective states, which can be obtained from the equation of continuity for the occupations. Here $\langle \dots \rangle$ denotes the quantum mechanical expectation value with the (nonequilibrium) distribution. Besides these one-particle density matrices $\langle a_{\beta}^{\dagger}(t) a_{\alpha}(t) \rangle$, higher order density matrices describe correlation effects and response functions.

Two formalisms exist to treat the quantum problem [i.e. to find approximations in order to obtain solutions for Eqs. (4,5)]: Within the method of density matrices, the temporal evolution of these quantities (where all operators are taken at the same time) is studied directly. This method was extremely successful in the study of electron kinetics on short time scales, see, e.g., Ref. [5] for details. On the other hand, Green functions depend on two different times. These have been used for stationary transport and for electron kinetics, see, e.g., Refs. [4,6] for details.

3 Method of Nonequilibrium Green Functions

The key quantities in the theory of nonequilibrium Green functions are the *correlation function* (or ‘lesser’ Green function)

$$G_{\alpha_1, \alpha_2}^{<}(t_1, t_2) = i \langle a_{\alpha_2}^{\dagger}(t_2) a_{\alpha_1}(t_1) \rangle \quad (6)$$

which describes the occupation of the states (for equal times and indices), together with the respective correlations both in time and state index, as well as the *retarded Green function*

$$G_{\alpha_1, \alpha_2}^{\text{ret}}(t_1, t_2) = -i \Theta(t_1 - t_2) \langle a_{\alpha_1}(t_1) a_{\alpha_2}^{\dagger}(t_2) + a_{\alpha_2}^{\dagger}(t_2) a_{\alpha_1}(t_1) \rangle \quad (7)$$

which describes the response of the system at time t_1 in state α_1 after an excitation at time t_2 in state α_2 .

If the external potential is static and transients resulting from initial conditions have disappeared, the system is typically in a stationary state¹ and all functions depend only on the time difference $t_1 - t_2$. Then it is convenient to work in Fourier space defined by

$$F_{\alpha_1, \alpha_2}(E) = \frac{1}{\hbar} \int dt e^{iEt/\hbar} F_{\alpha_1, \alpha_2}(t + t_2, t_2). \quad (8)$$

This defines the energy E which is *not* the level energy E_α of a certain state, but a new parameter, setting an absolute scale to compare energies of different states. Then the following equations determine the Green functions [1,4,8]:

$$(E - E_{\alpha_1}) G_{\alpha_1, \alpha_2}^{\text{ret/adv}}(E) - \sum_{\beta} U_{\alpha_1, \beta} G_{\beta, \alpha_2}^{\text{ret/adv}}(E) = \delta_{\alpha_1, \alpha_2} + \sum_{\beta} \Sigma_{\alpha_1, \beta}^{\text{ret/adv}}(E) G_{\beta, \alpha_2}^{\text{ret/adv}}(E) \quad (9)$$

$$G_{\alpha_1, \alpha_2}^<(E) = \sum_{\beta, \beta'} G_{\alpha_1, \beta}^{\text{ret}}(E) \Sigma_{\beta, \beta'}^<(E) G_{\beta', \alpha_2}^{\text{adv}}(E) \quad (10)$$

where the advanced Green function is just given by $G_{\beta, \alpha}^{\text{adv}}(E) = \left\{ G_{\alpha, \beta}^{\text{ret}}(E) \right\}^*$. These equations contain the self energies, which are typically functionals of the Green functions, and depend on the approximation chosen. To provide a glimpse of their structure, two examples are given here:

In the simple Born approximation, the retarded self energy for impurity scattering with scattering matrix elements $V_{\alpha_1, \beta}$ is given by:

$$\Sigma_{\alpha_1, \alpha_2}^{\text{ret}}(E) = \sum_{\beta} \langle V_{\alpha_1, \beta} V_{\beta, \alpha_2} \rangle_{\text{imp}} \frac{1}{E - E_{\beta} + i0^+} \quad (11)$$

where $\langle V_{\alpha_1, \beta} V_{\beta, \alpha_2} \rangle_{\text{imp}}$ denotes the averaging over all impurity configurations. A comparison with Fermi's golden rule gives $\Im\{\Sigma_{\alpha, \alpha}^{\text{ret}}(E_{\alpha})\} = -\hbar/2\tau_{\alpha}$, which relates the imaginary part of Σ^{ret} to the lifetime τ_{α} of the state.

In the self-consistent Born approximation, the lesser self-energy for phonon scattering reads

$$\begin{aligned} \Sigma_{\alpha_1, \alpha_2}^<(E) = & \sum_{\mathbf{p}, l} \sum_{\beta_1, \beta_2} M_{\alpha_1, \beta_1}^{\text{phon}}(\mathbf{p}, l) M_{\beta_2, \alpha_2}^{\text{phon}}(\mathbf{p}, l) \\ & \times \left[n_B(\hbar\omega_l(\mathbf{p})) G_{\beta_1, \beta_2}^<(E - \hbar\omega_l(\mathbf{p})) \right. \\ & \left. + [n_B(\hbar\omega_l(\mathbf{p})) + 1] G_{\beta_1, \beta_2}^<(E + \hbar\omega_l(\mathbf{p})) \right], \end{aligned} \quad (12)$$

¹ This is not necessarily the case as self-sustained oscillations or even chaotic behavior frequently occur in semiconductor systems at high electric fields [7].

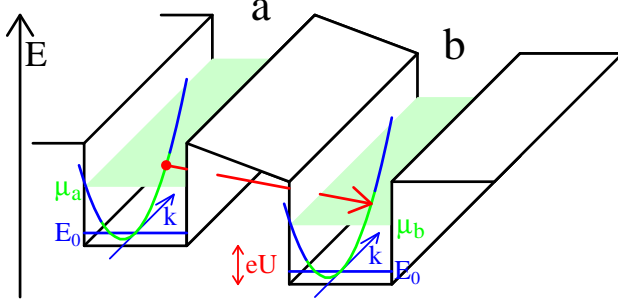


Fig. 1. Sketch of the test structure consisting of two neighboring quantum wells. A k -conserving transition is indicated

where $M_{\alpha_1, \beta_1}^{\text{phon}}(\mathbf{p}, l)$ is the matrix element of the electron-phonon interaction. \mathbf{p} and l denote the wave vector and the mode of the phonon spectrum with corresponding frequency $\omega_l(\mathbf{p})$. $n_B(E) = (\exp(E/k_B T) - 1)^{-1}$ is the Bose distribution, describing the occupation of phonon modes in thermal equilibrium. Taking into account that $G^<$ describes the occupation of states, one can identify the first term as phonon absorption from states with energy $E - \hbar\omega_l(\mathbf{p})$, and the second term as the combination of stimulated and spontaneous phonon emission from states with energy $E + \hbar\omega_l(\mathbf{p})$. This demonstrates that $\Sigma_{\alpha_1, \alpha_2}^<(E)$ is just the in-scattering rate at energy E . Furthermore it becomes clear, that E is the relevant energy scale for the occupation, and indeed in thermal equilibrium one finds

$$G_{\alpha, \alpha}^<(E) = iA_{\alpha}(E)n_F(E - \mu) \quad (13)$$

with the spectral function $A_{\alpha}(E) = -2\Im\{G_{\alpha, \alpha}^{\text{ret}}(E)\}$ and the electro-chemical potential μ . It is crucial to note, that the energy E enters the Fermi function $n_F(E - \mu)$ instead of the level energy E_{α} .

Eqs. (9,10) have to be solved self-consistently with the functionals for the self-energies, which is a formidable task. Finally, the physical observables of interest can be calculated via the density matrices

$$\langle a_{\beta}^{\dagger}(t)a_{\alpha}(t) \rangle = -i \int \frac{dE}{2\pi} G_{\alpha, \beta}^<(E). \quad (14)$$

Such calculations have been performed for the double barrier resonant tunneling diode [9] and superlattice structures [10,11]. In Section 6, simulation results for a quantum cascade laser structure are presented. In order to study the general concept, an analytic solution for a simple example will be given in the subsequent section.

4 A simple example

Let us consider sequential tunneling between two neighboring quantum wells, labeled by a and b , see Fig. 1. In both wells only the lowest bound state (with

energy E_0) plays a role and the in-plane behavior is determined by plane waves with quasimomentum $k = (k_x, k_y)$ and the dispersion $E_k = \hbar^2 k^2 / 2m$. Such an experiment has been performed by applying separate contacts to the individual layers [12,13]. Reflecting the experimental situation, the following assumptions are used in the theory:

- The translational invariance of the structure allows only for k -conserving transitions $a \rightarrow b$ with a tunneling matrix-element M .
- Due to weak coupling between the layers, only a small current is present, so that both layers are in thermal equilibrium with the respective contact.
- The electron densities in both layers are equal, so that the bias U determines both the difference in electro-chemical potentials $\mu_a - \mu_b = eU$, and the shift of the energy level b by $-eU$.
- Impurity scattering is the dominant scattering process, which is realistic for the case of vanishing temperature, $T \rightarrow 0$, considered here. Correlations in the impurity potential between both wells are neglected.

First note, that the simple application of Fermi's golden rule forbids transitions between the wells (see the arrow in Fig. 1) for $U \neq 0$, due to the energy conserving δ -function. Therefore a quantum transport calculation is indispensable. From the assumptions mentioned above we obtain the Hamiltonian

$$\begin{aligned} \hat{H} = & \sum_k (E_0 + E_k) a_k^\dagger a_k + (E_0 + E_k - eU) b_k^\dagger b_k + M b_k^\dagger a_k + M a_k^\dagger b_k \\ & + \sum_{k,k'} V_{k,k'}^a a_k^\dagger a_{k'} + V_{k,k'}^b b_k^\dagger b_{k'} \end{aligned} \quad (15)$$

where the matrix elements $V_{k,k'}^{a/b}$ for impurity scattering are subject to impurity averaging during the calculation.

Now we apply the Green function approach discussed in the last section. The general state index α is replaced by the two indices $a/b, k$. Neglecting correlations in the impurity potential between both wells implies $\langle V_{k,k'}^\mu V_{k',k}^\nu \rangle_{\text{imp}} \sim \delta_{\mu,\nu}$. Therefore the self-energies are diagonal in the well index and Eq. (9) takes the form

$$\begin{aligned} & \begin{pmatrix} G_{aa}^{\text{ret}}(k; E) & G_{ab}^{\text{ret}}(k; E) \\ G_{ba}^{\text{ret}}(k; E) & G_{bb}^{\text{ret}}(k; E) \end{pmatrix} \\ & = \begin{pmatrix} E - E_0 - E_k - \Sigma_{aa}^{\text{ret}}(k; E) & -M \\ -M & E - E_0 - E_k + eU - \Sigma_{bb}^{\text{ret}}(k; E) \end{pmatrix}^{-1} \end{aligned} \quad (16)$$

which gives $\mathbf{G}^{\text{ret}}(k; E) = \mathbf{G}^{\text{ret}(0)}(k; E) + M \mathbf{G}^{\text{ret}(1)}(k; E) + \mathcal{O}(M^2)$ with

$$G_{\mu\nu}^{\text{ret}(0)}(k; E) = \delta_{\mu\nu} \frac{1}{E - E_0 - E_k + eU \delta_{\nu,b} - \Sigma_{\nu\nu}^{\text{ret}}(k; E)} \quad (17)$$

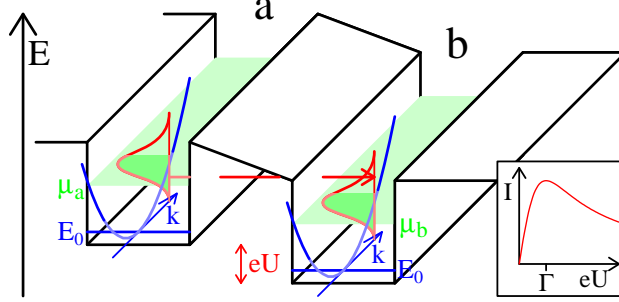


Fig. 2. Transitions in the Green-function treatment at fixed energy E . Transitions are allowed if $A_a(k, E)$ and $A_b(k, E)$ overlap in the energy window between the electrochemical potentials. The inset depicts the current-voltage characteristic

and

$$\mathbf{G}^{\text{ret}(1)}(k; E) = \begin{pmatrix} 0 & G_{aa}^{\text{ret}(0)}(k; E)G_{bb}^{\text{ret}(0)}(k; E) \\ G_{bb}^{\text{ret}(0)}(k; E)G_{aa}^{\text{ret}(0)}(k; E) & 0 \end{pmatrix} \quad (18)$$

Then Eq. (10) yields

$$G_{ba}^<(k; E) = G_{bb}^{\text{ret}(0)}(k; E)MG_{aa}^<(0)(k; E) + G_{bb}^<(0)(k; E)MG_{aa}^{\text{adv}(0)}(k; E) + \mathcal{O}(M^2) \quad (19)$$

The zeroth order terms refer to the uncoupled layers in equilibrium. Therefore Eq. (13) applies and with Eqs. (5,14) one obtains the total current [8]

$$I^{a \rightarrow b} = 2(\text{for Spin}) \frac{eM^2}{\hbar} \sum_k \int \frac{dE}{2\pi} A_a(k; E) A_b(k; E) \times [n_F(E - \mu_a) - n_F(E - \mu_b)] + \mathcal{O}(M^3). \quad (20)$$

This result shows that the transitions occur at fixed energy E , see Fig. 2. The spectral functions $A_a(k, E)$ and $A_b(k, E)$ give the weight of the levels a and b at the energy E , respectively. For each energy, there is a contribution to the current if there is a finite weight of both states and difference in occupation $[n_F(E - \mu_a) - n_F(E - \mu_b)]$. This demonstrates the crucial role of E as an energy scale. Following Sec. 3.3 of Ref. [11] this expression can be simplified for $\Sigma_{\nu\nu}^{\text{ret}}(k; E) = -i\Gamma/2$:

$$I_{GFT}^{a \rightarrow b} \approx A \frac{e|M|^2 \rho_0}{\hbar} \frac{2\Gamma}{(eU)^2 + \Gamma^2} \int dE [n_F(E - \mu_a) - n_F(E - \mu_b)] \quad (21)$$

where $\rho_0 = m/(\pi\hbar^2)$ is the two-dimensional density of states including spin and A is the sample area. Eq. (21) was used in the interpretation of the experiments [12,13] where good agreement was found.

5 Treatment by density matrices

For comparison, the example of the preceding section will now be treated within the density matrix approach. Here the key quantities are the occupations $f_a(k) = \langle a_k^\dagger a_k \rangle$ and $f_b(k) = \langle b_k^\dagger b_k \rangle$ as well as the polarisation $P(k) = \langle b_k^\dagger a_k \rangle$, which provides the transition rates according to Eq. (5). The key idea is to derive the temporal evolution of these quantities as a set of differential equations and to solve these after some approximations. Thus

$$\begin{aligned} \frac{\hbar}{i} \frac{d}{dt} P(k, t) &= \langle [\hat{H}, b_k^\dagger(t) a_k(t)] \rangle \\ &= -eU P(k, t) + M [f_a(k, t) - f_b(k, t)] \\ &\quad + \sum_{k'} \left[V_{k'k}^b \langle b_{k'}^\dagger(t) a_k(t) \rangle - V_{kk'}^a \langle b_k^\dagger(t) a_{k'}(t) \rangle \right] \end{aligned} \quad (22)$$

The density matrices $\langle b_k^\dagger(t) a_{k'}(t) \rangle$ contain the phase of the scattering matrix-element $V_{kk'}^a$. Thus one evaluates the temporal evolution as

$$\begin{aligned} \frac{\hbar}{i} \frac{d}{dt} V_{kk'}^a \langle b_k^\dagger(t) a_{k'}(t) \rangle &= (E_k - eU - E_{k'}) V_{kk'}^a \langle b_k^\dagger a_{k'} \rangle \\ &\quad + M \left[V_{kk'}^a \langle a_k^\dagger a_{k'} \rangle - V_{kk'}^a \langle b_k^\dagger b_{k'} \rangle \right] \\ &\quad + \sum_{\mathbf{k}''} V_{k''k}^b V_{kk'}^a \langle b_{k''}^\dagger a_{k'} \rangle - \sum_{\mathbf{k}''} V_{kk'}^a V_{k''k'}^a \langle b_k^\dagger a_{k''} \rangle \end{aligned} \quad (23)$$

After impurity averaging one finds $\langle V_{k''k}^\nu V_{kk'}^a \rangle_{\text{imp}} = |V_{kk'}^a|^2 \delta_{\nu a} \delta_{k'', k'}$ and we have

$$\begin{aligned} \frac{\hbar}{i} \frac{d}{dt} V_{kk'}^a \langle b_k^\dagger(t) a_{k'}(t) \rangle &= (E_k - eU - E_{k'}) V_{kk'}^a \langle b_k^\dagger a_{k'} \rangle - |V_{kk'}^a|^2 P(k, t) \\ &\quad + M \left[V_{kk'}^a \langle a_k^\dagger a_{k'} \rangle - V_{kk'}^a \langle b_k^\dagger b_{k'} \rangle \right] \end{aligned} \quad (24)$$

In Eq (24) it is tempting to neglect the last line, as these terms contain both M and V . In this case one obtains

$$V_{kk'}^a \langle b_k^\dagger(t) a_{k'}(t) \rangle = \frac{1}{E_k - eU - E_{k'} + i0^+} |V_{kk'}^a|^2 P(k) \quad (25)$$

in the stationary state, where the term $i0^+$ ensures that correlations vanish for $t \rightarrow -\infty$. Therefore

$$\sum_{k'} V_{kk'}^a \langle b_k^\dagger(t) a_{k'}(t) \rangle = \Sigma_a^{\text{ret}}(k, E_0 + E_k - eU) P(k) \quad (26)$$

where Eq. (11) has been used. In the same way one finds $\sum_{k'} V_{k'k}^b \langle b_{k'}^\dagger(t) a_k(t) \rangle = \Sigma_b^{\text{adv}}(k, E_0 + E_k) P(k)$. Inserting into Eq. (22) gives the polarisation

$$P(k) = \frac{M [f_a(k) - f_b(k)]}{eU + \Sigma_a^{\text{ret}}(k, E_0 + E_k - eU) - \Sigma_b^{\text{adv}}(k, E_0 + E_k)} \quad (27)$$

and with $\Sigma_b^{\text{adv}}(k, E_0 + E_k) - \Sigma_a^{\text{ret}}(k, E_0 + E_k - eU) \approx i\Gamma$ the current

$$I_{\text{DMTsimp}}^{a \rightarrow b} = 2(\text{for Spin})e \frac{M^2}{\hbar} \sum_k \frac{2\Gamma}{(eU)^2 + \Gamma^2} [f_a(k) - f_b(k)] . \quad (28)$$

This means that the transitions occur between states with the same k as indicated in Fig. 1. In contrast to the treatment by Fermi's golden rule, lifetime broadening allows for these transitions even for finite U . This structure appears frequently in density matrix calculations, see, e.g., Ref. [14] for sequential tunneling. On first sight $I_{\text{DMTsimp}}^{a \rightarrow b}$ seems to be similar to $I_{\text{GFT}}^{a \rightarrow b}$. But for the situation considered, $I_{\text{DMTsimp}}^{a \rightarrow b}$ vanishes, because $f_a(k) \equiv f_b(k)$ as the electron density is identical in both wells. This indicates that the result is not trustworthy.

Now we take into account the first term in the last line of Eq (24), which indeed is of the same order as the other terms because $P(k)$ is of order M . Therefore we have to evaluate

$$\begin{aligned} \frac{\hbar}{i} \frac{d}{dt} V_{kk'}^a \langle a_k(t)^\dagger a_{k'}(t) \rangle &= (E_k - E_{k'}) V_{kk'}^a \langle a_k^\dagger a_{k'} \rangle \\ &+ M \left[V_{kk'}^a \langle b_k^\dagger a_{k'} \rangle - V_{kk'}^a \langle a_k^\dagger b_{k'} \rangle \right] \\ &+ \sum_{k''} V_{k''k}^a V_{kk'}^a \langle a_{k''}^\dagger a_{k'} \rangle - V_{kk'}^a V_{k''k'}^a \langle a_k^\dagger a_{k''} \rangle \end{aligned} \quad (29)$$

Performing impurity averaging and neglecting the M terms (yielding expressions of order M^2) gives:

$$V_{kk'}^a \langle a_k(t)^\dagger a_{k'}(t) \rangle = \frac{-1}{E_k - E_{k'} + i0^+} |V_{kk'}^a|^2 [f_a(k') - f_a(k)] \quad (30)$$

Now the solution of Eq (24) provides

$$\begin{aligned} V_{kk'}^a \langle b_k^\dagger(t) a_{k'}(t) \rangle &= \frac{1}{E_k - eU - E_{k'} + i0^+} |V_{kk'}^a|^2 P(k) \\ &+ \frac{M}{eU} \left[\frac{1}{E_k - eU - E_{k'} + i0^+} - \frac{1}{E_k - E_{k'} + i0^+} \right] \\ &\times |V_{kk'}^a|^2 [f_a(k') - f_a(k)] . \end{aligned} \quad (31)$$

Using $\Im\{1/(x + i0^+)\} = -\pi\delta(x)$ and neglecting the corresponding real part one obtains

$$\begin{aligned} \sum_{k'} V_{kk'}^a \langle b_k^\dagger(t) a_{k'}(t) \rangle &\approx \Sigma_a^{\text{ret}}(k, E_0 + E_k - eU) P(k) \\ &+ i \frac{M}{eU} \Im\{\Sigma_a^{\text{ret}}(k, E_0 + E_k - eU)\} [n_a(E_k - eU) - n_a(E_k)] \end{aligned} \quad (32)$$

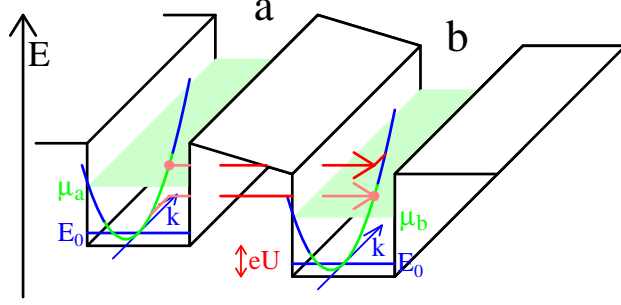


Fig. 3. Transitions in the density matrix treatment according to Eq. (34). The current is driven by impurity assisted transitions between states of different k , so that the energy is conserved

where $n_a(E_k) = f_a(k)$. In the same way one obtains

$$\begin{aligned} \sum_{k'} V_{k'k}^b \langle b_{k'}^\dagger(t) a_k(t) \rangle &\approx \Sigma_b^{\text{adv}}(k, E_0 + E_k) P(k) \\ &+ i \frac{M}{eU} \Im \{ \Sigma_b^{\text{adv}}(k, E_0 + E_k) \} [n_b(E_k) - n_b(E_k + eU)] \end{aligned} \quad (33)$$

Inserting into Eq. (22) and using $\Sigma^{\text{adv/ret}} \approx \pm i\Gamma/2$ one obtains after a few lines of algebra

$$\begin{aligned} I_{\text{DMT}}^{a \rightarrow b} &= 2e \frac{M^2}{\hbar} \sum_k \frac{2\Gamma}{(eU)^2 + \Gamma^2} \\ &\times \left[\frac{n_a(E_k) - n_b(E_k + eU)}{2} + \frac{n_a(E_k - eU) - n_b(E_k)}{2} \right] \end{aligned} \quad (34)$$

This means, that the current is driven by the difference in occupation at the same energy, rather than the difference in occupation at the same k . Fig. 3 suggests that these transitions should be viewed as scattering-assisted transitions. Note, that this interpretation is completely different from the result by Eq. (28). The fact, that the transitions occur at fixed energy strongly resembles the Green-function formalism, see Fig. 2, and the evaluation of Eq. (21) and Eq. (34) give similar results. The difficulty in obtaining this result in density matrix theory seems to be related to the fact that, unlike in the Green function formalism, the energy scale E is not available.

6 Results for quantum cascade laser structures

Electrically driven unipolar semiconductor lasers can be made by a proper design of nanostructures. The key point is population inversion between subbands, which can be achieved by a rather complicated sequence of quantum wells. In order to amplify this effect, several periods of such sequences are grown on top of each other, resulting in a quantum cascade laser [15] operating in the 10 μm range.

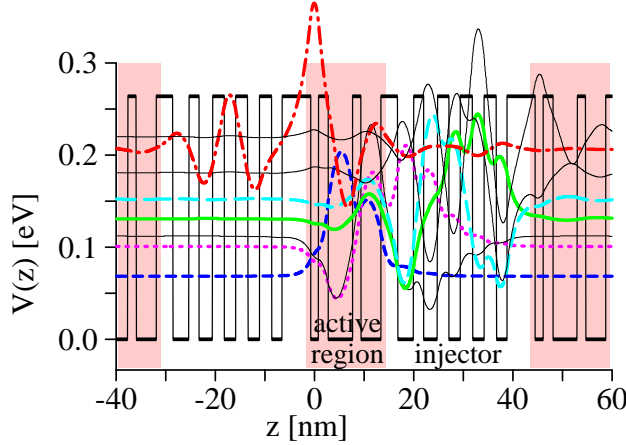


Fig. 4. Conduction band of the quantum cascade laser structure from Ref. [16]. The eight lowest Wannier functions are given for one period, where the base line depicts the respective level energy. Note that these functions are repeated in each period

In Fig. 4 such a structure (from Ref. [16]) is shown. Here one period consists of an active region (where the lasing transition occurs) of 3 wells ($0 < z < 15$ nm) and the injector region of 5 wells (for $15\text{nm} < z < d$). This sequence with period $d = 45.3$ nm is repeated 30 times in the experiment.

Similar to the treatment in Section 4, we use a set of basis states consisting of localized states in the growth direction (labeled by ν) and a free particle behavior with wave vector k perpendicular to the growth direction. For the localized states we use Wannier functions as depicted in Fig. 4. This allows for a calculation of all matrix elements in Eqs. (2,3) from the sample parameters following Ref. [11]. For field strengths of the order of $F \approx 50$ kV/cm, the states in the injector become aligned to the excited state (dashed-dotted line) in the active region of the next period. This design provides a strong enhancement of population of this level associated with with population inversion in the active region.

The self-energies are evaluated within the self-consistent Born approximation treating scattering with impurities, optic phonons, and acoustic phonons similar to Ref. [11]. Eqs. (9,10) were solved self-consistently with the functionals for the self-energies reaching an accuracy of approximately 1%. Details will be given elsewhere [17]. For practical purposes the momentum dependence of the matrix elements had to be neglected. Thus, these quantum transport calculations can be considered as complementary to semiclassical Monte-Carlo simulations [18,19], where such details can be easily taken into account.

Fig. 5 shows some results from our calculations. The field-current relation is in good agreement with the experimental findings of Ref. [16]. The electron densities of level ν are evaluated by

$$n_\nu = \frac{2(\text{for spin})}{A} \sum_k \int \frac{dE}{2\pi} \Im\{G_{\nu\nu}^<(k; E)\}. \quad (35)$$

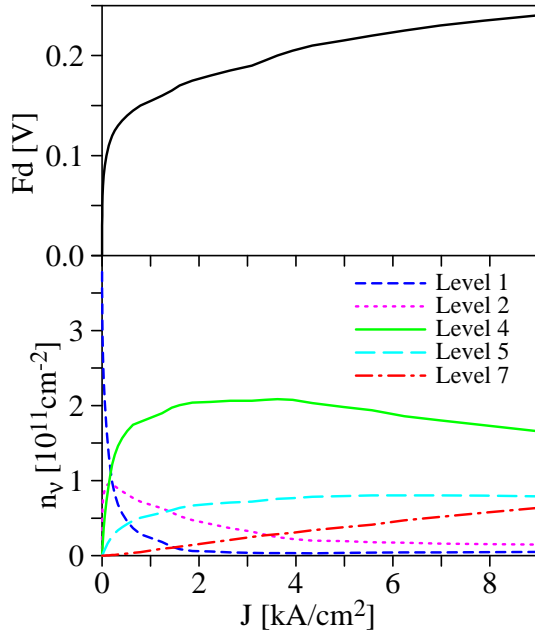


Fig. 5. Voltage drop per period Fd as well as occupation n_v for different levels versus current density. The linestyle corresponds to the fat lines in Fig. 4. The occupation of the other levels is below $5 \times 10^{10}/\text{cm}^2$ for all currents

For vanishing current and field, essentially the lowest level is occupied. With increasing field, the energy of the levels 4, 5, and 6 is diminished because they are located further to the right. Thus, the carriers are transferred to these states, which are located in the injector region. At the same time the occupation of level 7 increases linearly with the current, which indicates that the transport essentially occurs via this level. (The sample was designed precisely for this behavior.) At moderate currents, occupation inversion occurs between this level 7 and the levels 1, 2, and 3, which are lower in energy. As the dipole matrix element between these levels and level 7 is rather large (all of them are essentially located in the active region), lasing is likely to occur, which is indeed observed in the device for current densities above $7 \text{ kA}/\text{cm}^2$.

7 Conclusion

Nonequilibrium Green functions provide a powerful tool to study quantum transport in nanostructures under stationary conditions. They allow for a quantitative description of nanostructure devices such as superlattices and quantum cascade lasers. The power of this method results from the availability of the global energy scale E , the frequency related to the time difference in $G(t_1, t_2)$. Although essentially the same results can be obtained in density matrix theory, the structure of the equations appear more complicated there.

Fruitful cooperation with S.-C. Lee and financial support by DFG within SFB296 and FOR394 are gratefully acknowledged.

References

1. S. Datta: *Electronic Transport in Mesoscopic Systems* (Cambridge University Press, Cambridge, 1995).
2. D. K. Ferry and S. M. Goodnick: *Transport in Nanostructures* (Cambridge University Press, Cambridge, 1997).
3. T. Dittrich, P. Hänggi, G.-L. Ingold, B. Kramer, G. Schön, and W. Zwerger: *Quantum Transport and Dissipation* (Wiley-VCH, Weinheim, 1998).
4. H. Haug and A.-P. Jauho: *Quantum Kinetics in Transport and Optics of Semiconductors* (Springer, Berlin, 1996).
5. T. Kuhn: in *Theory of Transport Properties of Semiconductor Nanostructures*, edited by E. Schöll (Chapman and Hall, London, 1998).
6. M. Bonitz (Ed.): *Progress in Nonequilibrium Green's Functions* (World Scientific, Singapore, 2000).
7. E. Schöll: *Nonlinear spatio-temporal dynamics and chaos in semiconductors* (Cambridge University Press, Cambridge, 2001).
8. G. D. Mahan: *Many-Particle Physics* (Plenum, New York, 1990).
9. R. Lake, G. Klimeck, R. C. Bowen, and D. Jovanovic: J. Appl. Phys. **81**, 7845 (1997).
10. A. Wacker, A.-P. Jauho, S. Rott, A. Markus, P. Binder, and G. H. Döhler: Phys. Rev. Lett. **83**, 836 (1999).
11. A. Wacker: Phys. Rep. (2001), in press.
12. S. Q. Murphy, J. P. Eisenstein, L. N. Pfeiffer, and K. W. West: Phys. Rev. B **52**, 14825 (1995).
13. N. Turner, J. T. Nicholls, E. H. Linfield, K. M. Brown, G. A. C. Jones, and D. A. Ritchie, Phys. Rev. B **54**, 10614 (1996).
14. R. F. Kazarinov and R. A. Suris: Sov. Phys. Semicond. **6**, 120 (1972), [Fiz. Tekh. Poluprov. **6**, 148 (1972)].
15. J. Faist, C. Sirtori, F. Capasso, L. Pfeiffer, and K. W. West: Appl. Phys. Lett. **64**, 872 (1994).
16. C. Sirtori, P. Kruck, S. Barbieri, P. Collot, J. Nagle, M. Beck, J. Faist, and U. Oesterle: Appl. Phys. Lett. **73**, 3486 (1998).
17. S.-C. Lee and A. Wacker: in preparation.
18. S. Tortora, F. Compagnone, A. Di Carlo, P. Lugli, M. T. Pellegrini, M. Troccoli, and G. Scamarcio: Physica B **272**, 219 (1999).
19. R. C. Iotti and F. Rossi: Appl. Phys. Lett. **76**, 2265 (2000).